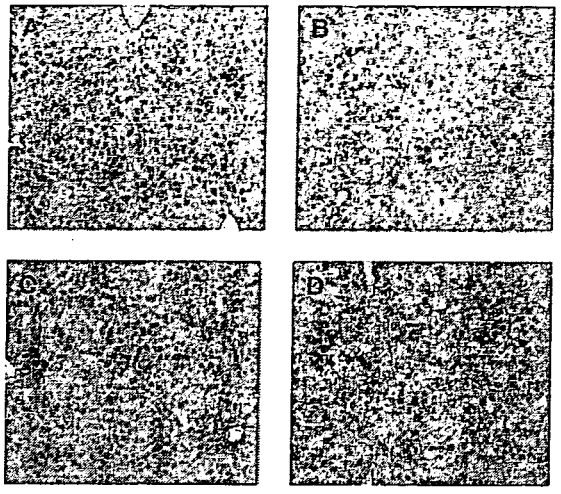

Figure 3. Microscopic images of the liver following conventional or hydrodynamic injection. Mice were treated with 0.2 ml of saline by conventional injection (A) or with 2 ml of saline containing 0 (B), 1 (C) or 10% (w/v) (D) PEG2000 using the hydrodynamic injection. At 10 min after each injection, the liver was removed, fixed in 20% neutral-buffered formalin, sectioned at 5 μm and stained with hematoxylin and eosin. Magnification 50×

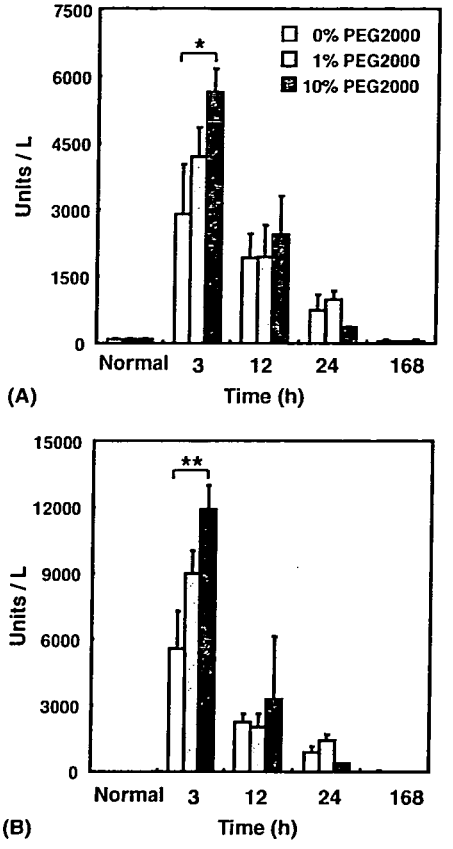

Figure 4. Profiles of serum enzymes (AST (A) and ALT (B)) following the hydrodynamic injection. Mice received a large-volume intravenous injection of saline (2 ml/mouse/5 s) and blood was collected at the indicated times. Serum AST and ALT activities were determined. Normal represents age-matched, untreated mice. The results are expressed as the mean ± S.D. (n = 3). Statistical significance between gene expression levels with different PEG concentrations (0, 1 and 10%) was analyzed by one-way ANOVA. $^{*}p < 0.05$; $^{**}p < 0.01$

the cytoplasm displaying decreased basophilia as well as a fine granular appearance and necrobiosis, sometimes with erythrocytes in the cytoplasm. The histopathological scores are summarized in Table 1. Hydrodynamics-based injection with 1% (w/v) PEG2000 caused significantly less liver damage than the hydrodynamics injection with none or 10% (w/v) PEG2000.

Hepatocyte damage was also determined by measurement of serum levels of the liver enzymes aspartate aminotransferase (AST) and alanine aminotransferase (ALT). Figure 4 shows the concentration profiles of AST and ALT following the hydrodynamic injection with none, 1% (w/v) or 10% (w/v) PEG2000. In this study, we excluded time points less than 3 h, after injection, because of the extensive blood dilution by the large volume of injected solution. We observed a strong but transient elevation of liver enzymes following hydrodynamic injection, dependent on PEG concentration. The highest levels were detected 3 h after injection. Enzyme levels then decreased gradually and returned to normal by 168 h (7 days). Surprisingly, the hydrodynamic injection with 1% (w/v) PEG2000 showed no significant difference in the level of ALT and AST compared to the hydrodynamic injection without PEG.

Quantification of pDNA transported into hepatocytes and nuclei as a result of hydrodynamic injection

The amount of pDNA delivered into the hepatocytes or their nuclei was determined by PCR at 12 and 24 h

Table 1. Histopathological observations after hydrodynamic injection with various concentrations of PEG2000

	Histopathological scores											
Injection group	Conventional injection (200 μl)			Hydrodynamic injection (2 ml)								
PEG concentration (% (w/v))	–			0			1			10		
Grade	+	++	+++	+	++	+++	+	++	+++	+	++	+++
Number of mice ($n = 5$)	0	0	0	0	1	4	0	3	2	0	0	5

The histopathological scores were recorded by microscopic examination of liver sections as described in Figure 3. +: slight, ++: moderate, +++: severe.

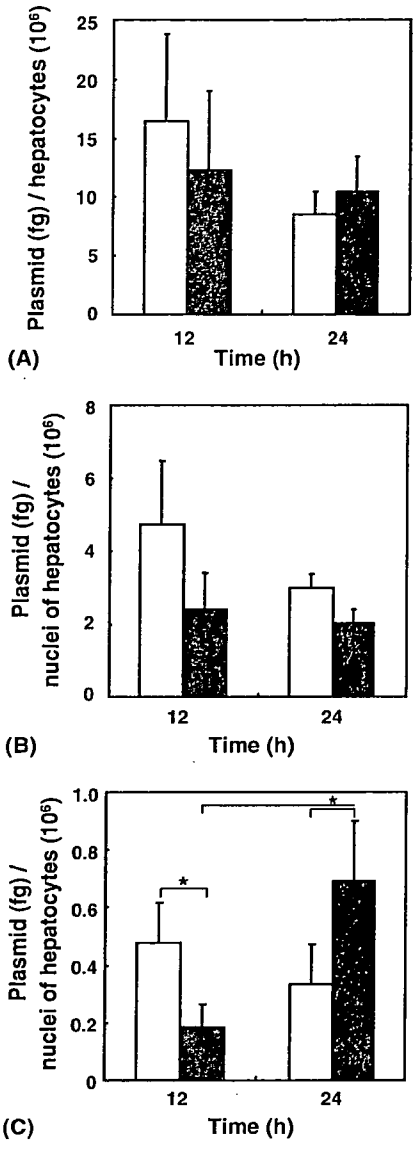

Figure 5. Total amount of pDNA delivered to hepatocytes (A) or to hepatocyte nuclei (B) or intact pDNA delivered to hepatocyte nuclei (C) following hydrodynamic injection. The amount of pDNA delivered into the hepatocytes or nuclei of the hepatocytes was determined at 12 or 24 h after hydrodynamic injection of 40 μg pDNA with or without 1% (w/v) PEG2000. The amount of intact pDNA transported into the nuclei of the hepatocytes was also determined. The results are expressed as the mean ± S.D. (n = 3). Statistical significance was analyzed by Dunnett's test. $^*p < 0.05$

after the injection. With the hydrodynamic injection method substantial amounts of pDNA were transported into hepatocytes (Figure 5A). By contrast, with the conventional injection method, pDNA levels in the hepatocytes were below the detection limit (data not shown). Although at 24 h pDNA levels in hepatocytes were somewhat lower than at 12 h, this difference was not significant (Figure 5A). Approximately 20–30% of the pDNA in the hepatocytes was transported in the nuclei (Figure 5B). There was no statistically significant difference between the 12 and 24 h time points, although pDNA transported by the hydrodynamic injection without PEG tended to decrease.

Since, obviously, only intact intranuclear pDNA reflects gene expression, it is necessary to distinguish between intact and partially or completely degraded DNA. Thus, we also determined only intact pDNA transported in the nuclei as a consequence of the hydrodynamic injection. At the earlier time point (12 h), the regular hydrodynamic injection, i.e. without PEG, transported a larger amount of intact pDNA in the nuclei than the hydrodynamic injection with PEG ($p < 0.05$) (Figure 5C). The amount of intact pDNA transported into the nuclei by the regular hydrodynamic injection did not change with time, but the amount transported by the hydrodynamic injection with PEG increased approximately 3.5-fold between 12 and 24 h. The fraction of intact pDNA as a percentage of total pDNA in the nuclei was 10.3 ± 0.7% at 12 h and 10.8 ± 3.7% at 24 h ($p = 0.85$), following the hydrodynamic injection without PEG. These values were 7.8 ± 1.4% at 12 h and 38.4 ± 13.7% at 24 h ($p < 0.05$), following the hydrodynamic injection with PEG.

Time-course study on gene expression in the liver induced by the improved hydrodynamics-based procedure

The results described above indicate that our modified hydrodynamics-based procedure, i.e. a rapid injection of a large volume of 1% (w/v) PEG2000-containing pDNA solution, may enhance gene expression relative to that achieved by the regular hydrodynamics-based procedure. To examine this possibility, a time-course study on the expression of luciferase in the liver was carried out following the injection (Figure 6). In the regular hydrodynamic injection, luciferase activity reached a maximum level at 8–12 h. From then on the level gradually decreased by 72 h. Our modified hydrodynamics-based procedure moved the peak of maximum luciferase activity to 24 h and increased the maximum level nearly 2-fold compared to the regular procedure. From then on the expression was gradually decreased, but the level at 72 h was still much higher (approximately 300-fold) than that of the regular hydrodynamic injection. The area under the gene expression-time curve was enlarged approximately 2-fold by addition of 1% (w/v) PEG2000. Clearly, the addition of PEG2000 substantially enlarged the hepatic gene expression induced by the hydrodynamics-based procedure as we expected.

Discussion

The liver is an important target organ for gene transfer due to its large capacity for synthesizing serum proteins and its involvement in numerous genetic and acquired diseases. Thus, liver-targeted gene transfer is an important tool for expanding the treatment options for liver

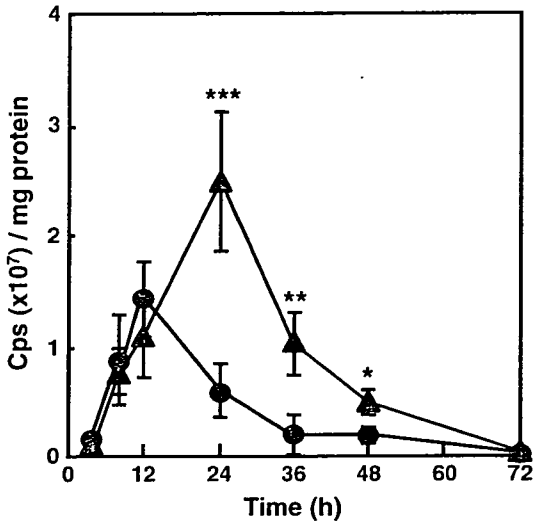

Figure 6. Profiles of gene expression in the liver following hydrodynamic injection. Mice received a large-volume intravenous injection of saline (40 μg pDNA in 2 ml/mouse/5 s) with or without 1% (w/v) PEG2000 and livers were processed for luciferase assay at the indicated times after the injection. ●; hydrodynamic injection without PEG (regular hydrodynamic injection), ▲; hydrodynamic injection with 1% PEG. Luciferase activities are expressed as mean ± S.D. (n = 6). Statistical significance against regular hydrodynamic injection was analyzed by Student's *t*-test. $^{*}p < 0.05$; $^{**}p < 0.01$; $^{***}p < 0.005$

diseases and diseases affecting other organ systems, and for gene function studies. Among the various gene delivery systems available, naked pDNA-mediated gene transfer is the simplest, and techniques for introducing naked pDNA into hepatocytes have been among the most intensely studied methods to generate therapeutic amounts of gene product. Liu *et al.* [11] and Zhang *et al.* [5] have developed a technique that does not require local administration or surgical procedures, to produce extremely high expression levels of exogenous genes in mouse liver, using the systemic rapid administration with a large volume of naked pDNA solutions into the tail vein. However, in these reports, the induced gene expression was transient, probably because introduced pDNA was rapidly degraded in the hepatocytes and/or transfected hepatocytes were removed by the immune system. Our study indicates that enhanced gene expression levels in mouse liver can be achieved by addition of only 1% (w/v) PEG2000 to a large volume of pDNA solution and subsequent hydrodynamic injection. This modified simple gene transfer method would increase the potential of the regular hydrodynamics-based procedure for laboratory studies and gene therapy, although further studies will be required to understand the mechanism whereby enhancement of gene expression is achieved before application to other tissues or to humans can be considered.

Based on serum enzyme and histological examinations (Figures 2, 3, and 4), the hydrodynamic injection procedure clearly induces transient damage against the hepatocytes, irrespective of the presence of PEG2000. The liver damage was not the result of pDNA delivery, but rather a reaction to the vehicle or procedure, since injection of saline induced similar damage on the liver (data not shown). It is likely that the PEG2000 causes the liver damage to further escalate in a PEG-concentration-dependent manner, since the level of serum enzymes increased with an increase in the PEG concentration (Figure 4). This PEG-induced escalation of damage brings with it a concern that the PEG2000 increases the toxicity of the regular procedure. However, no significant additional liver damage was caused by addition of 1% (w/v) PEG2000 (Table 1, Figures 3 and 4), compared to that by the regular hydrodynamic injection. Liu *et al.* [11] found no indication of serious liver damage as assessed by animal growth and clinical biochemistry tests, which were all in normal range with the exception of a transient increase in serum concentration of alanine aminotransferase. Currently, there is an increasing interest in the usefulness of PEG for biomedical applications, particularly because of its relative low toxicity and rapid clearance by urinary excretion. Concentrations of PEG up to 40% (w/v) are considered safe and relatively nontoxic for use in animal studies [36]. This suggests that our procedure as described here, hydrodynamic injection with 1% (w/v) PEG2000, is safe for animals, and the procedure is acceptable and useful for analyzing regulation of gene expression *in vivo*, although further safety investigations will be required.

Interestingly, the PEG concentration was inversely related to the level of gene expression in the liver (Figure 1). It appears that the PEG plays a bifunctional role in gene expression following the hydrodynamic injection, i.e. it increases gene expression at lower concentration, whereas it diminishes it at higher concentration. Very similar results were reported on gene delivery in skeletal muscles with the block copolymers SP1017 and PE6400 [37,38]. At low concentrations (up to 0.01% (w/v) for SP1017 and 0.5% (w/v) for PE6400), gene expressions were increased in a dose-dependent manner. At higher concentrations, the efficacy of gene expression declined. Although the mechanism of the bifunctionality of block copolymers on gene transfer remains to be explored, that of PEG observed here probably results from the PEG-concentration-dependent liver damage observed in Figures 3 and 4. Death of a large number of hepatocytes would cause gene expression in very few labile hepatocytes, if the PEG enhanced the delivery of a large amount of pDNA to the hepatocytes relative to the regular hydrodynamics-based procedure.

Two mechanisms have been proposed to explain the entry of pDNA into hepatocytes following the hydrodynamic injection: endocytosis [39] or penetration by plasma membrane pores created by the hydrodynamic pressure [40]. According to recent reports [41,42], the second mechanism is more likely. PEG has a variety of effects on biological systems [23–26]. One of them is to increase membrane permeability due to osmotic effects [30]. We expected that the addition of PEG to the hydrodynamic injection solution would increase membrane permeability of hepatocytes and thereby

elevate the amount of pDNA transported intracellularly, resulting in enhanced gene expression in the hepatocytes. Our results showed that the PEG did enhance gene expression in the liver (Figures 1 and 6). However, this is not a result of an increased amount of pDNA transported to the hepatocytes, as revealed by Figure 5B. This figure suggests that the PEG does not affect the process facilitating the entry of pDNA into the hepatocytes, which is supported by our experiment with Evans Blue dye injection showing that the PEG did not affect the membrane permeability of hepatocytes due to the hydrodynamic injection (Figure 2).

Once the pDNA molecules have entered into the hepatocytes, they must be transported to the nucleus, where transcription takes place, to cause efficient gene expression. This process is considered one of the limiting steps governing the efficiency of gene expression. As mentioned above, both hydrodynamic procedures transported similar amounts of pDNA to the nuclei (Figure 5B). However, in terms of *intact* pDNA, the addition of PEG clearly increased the amount in the nuclei with increasing time after injection (the regular procedure, $10.8 \pm 3.7\%$ (intact pDNA to total pDNA, at 24 h) vs. our procedure, $38.4 \pm 13.7\%$, ($p < 0.05$), estimated from the results in Figures 5B and 5C). This efficient transport of *intact* pDNA to the nuclei may account for the enhancement of gene expression (Figures 1 and 6). The mechanism by which PEG elevates the amount of *intact* pDNA in the nuclei is unclear. It may involve in part cytosolic delivery of PEG via an influx along with the large volume of pDNA solution. Presumably then, the infused PEG prevents pDNA molecules from degradation by the intracellular DNases, resulting in retention of a large number of *intact* pDNA copies intracellularly. As a result, transport of intracellular *intact* pDNA to nuclei may be facilitated efficiently with increasing the time after the injection.

Recent observations by Andrianaivo *et al.* [42] may provide another possible mechanism by which PEG may account for the enhanced transport of *intact* pDNA to nuclei. They showed that a large amount of pDNA remains bound to the outside of the plasma membrane of hepatocytes for a relatively long time after a hydrodynamic injection. The authors hypothesized that the hydrodynamics-based transfection takes place in two phases. In the first one a few DNA molecules entering the hepatocytes very quickly lead to a strong expression in a relatively short time. In the second one the DNA molecules bound to the plasma membrane cause a low expression for a long time via the relatively slow endocytosis process. On the basis of their hypothesis, the second process may be reinforced with the PEG in our study. It is likely that the PEG protects the pDNA bound to the plasma membrane from degradation by DNase and consequently enhances delivery of a relatively large number of pDNA molecules inside the hepatocytes. As a consequence, the intracellular source of intact pDNA for intranuclear transport may be maintained for a relatively long time.

It has been shown that the osmotic pressure of PEG affects the regulation of a number of physiological processes of cells. Both hypo- as well as hyperosmotic shocks induce changes in plant cell metabolism [43,44]. Cells have specific mechanisms for the restoration of their volume after osmotic shocks, involving the activation of tyrosine kinases [45]. Cell volume changes have been suggested to be of importance in the regulation of protein degradation and synthesis [46]. The increased activity of ornithine decarboxylase in osmotically swollen cells is at least partially related to an enhanced synthesis of the enzyme protein in the absence of a change in its mRNA production [47]. Transcription of specific genes in mammalian cells is enhanced by hypersmotic shock [48,49]. Taken together, the PEG in the large-volume pDNA solution may affect the physiological processes of hepatocytes after the hydrodynamic injection. The physiological change of the hepatocytes, along with a large number of *intact* pDNA molecules in the nuclei, may result in enhancement of gene expression in the liver, following the injection.

Recently, it was demonstrated that Pluronic block copolymers can increase regional expression of the naked pDNA after its injection in the skeletal and cardiac muscles [37,38,50]. The mechanism by which Pluronic block copolymer acted on the naked pDNA expression has not been established; however, the following speculations were made: (1) Interactions between the block copolymer and membrane accelerate cellular uptake of naked pDNA; (2) the block copolymer enhances pDNA distribution through muscle tissues; (3) the block copolymer may increase the transport of free pDNA from the cytoplasm to the nucleus of muscle cells; and (4) the block copolymer acts as synthetic biological response modifier, resulting in increased gene expression as a consequence of activating transcription of the gene. Taken together with these speculations and our results described here, the PEG may increase the transport of free pDNA from the cytoplasm to the nucleus of hepatocytes as well as activate the transcription of the transgene expression. However, at present, we cannot exclude the possibility that the infused PEG may also protect pDNA-derived mRNA or expressed exogenous protein (luciferase) from digestion by intracellular DNase or proteinases.

It is noteworthy that the vascular and/or hepatocyte-membrane permeability increased with increasing the time interval (up to 30 min) between hydrodynamic injection and Evans Blue injection (conventional injection) (Figure 2). This indicates that the enlargement of the liver endothelial fenestrae and hepatocyte-membrane defects remain in existence for at least 30 min after the hydrodynamic injection. In contrast, Zhang *et al.* [31] recently showed that most of the defects of the hepatocyte membranes resealed within 10 min after hydrodynamic injection. In addition, these defects have to disappear rapidly, as living cells have to reseal within seconds to a minute in order to survive [51]. This discrepancy may be due to the difference in experimental conditions. We

determined the level of Evans Blue in the liver by extraction of the dye directly from the liver tissue, while Zhang *et al.* assessed the microdistribution of the dye in the liver section by fluorescence microscopy. Under our conditions, all Evans Blue dye in the liver was quantitatively determined. This amount includes not only the dye entering the hepatocytes through the pores generated by the elevated pressure, but also that accumulating in Disse's space or Kupffer cells because the dye associates with serum albumin (Figure 3).

Despite many desirable features associated with our procedure, such as simplicity, convenience and high efficiency, the level and time of gene expression driven by our method may be yet too low and short. Recently, Herweijer *et al.* [52] reported the effect of a liver-specific promoter on longevity of transgene expression: the albumin promoter (a 300 bp promoter in conjunction with a 2 kb upstream enhancer region) sustained expression of luciferase in the liver following hydrodynamics-based transfection. Miao *et al.* [53] also reported a similar result that long-term expression of human factor IX in mice was achieved by tail vein injection of a pDNA employing an α 1-antitrypsin promoter in conjunction with a hepatic control region. Therefore, we are now testing whether high-level, sustained transgene expression in the liver can be achieved by using a pDNA containing liver-specific promoters with our method.

Acknowledgements

The authors thank Kenji Irimura of the Drug Safety Research Laboratory, Taiho Pharmaceutical Co., Ltd., for his excellent technical assistance with the histopathological examination. We wish to thank Dr. G. L. Scherphof for his helpful advice in writing the English manuscript. This work was supported in part by a Grant-in-Aid for Scientific Research from the Ministry of Education, Culture, Sports, Science and Technology, Japan.

References

1. Wolff JA, Malone RW, Williams P, *et al.* Direct gene transfer into mouse muscle in vivo. *Science* 1990; **247**: 1465–1468.
2. Hickman MA, Malone RW, Lehmann-Bruinsma K, *et al.* Gene expression following direct injection of DNA into liver. *Hum Gene Ther* 1994; **5**: 1477–1483.
3. Budker V, Zhang G, Knechtle S, *et al.* Naked DNA delivered intraportally expresses efficiently in hepatocytes. *Gene Ther* 1996; **3**: 593–598.
4. Zhang G, Vargo D, Budker V, *et al.* Expression of naked plasmid DNA injected into the afferent and efferent vessels of rodent and dog livers. *Hum Gene Ther* 1997; **8**: 1763–1772.
5. Zhang G, Budker V, Wolff JA. High levels of foreign gene expression in hepatocytes after tail vein injections of naked plasmid DNA. *Hum Gene Ther* 1999; **10**: 1735–1737.
6. Meyer KB, Thompson MM, Levy MY, *et al.* Intratracheal gene delivery to the mouse airway: characterization of plasmid DNA expression and pharmacokinetics. *Gene Ther* 1995; **2**: 450–460.
7. Li K, Welikson RE, Vikstrom KL, *et al.* Direct gene transfer into the mouse heart. *J Mol Cell Cardiol* 1997; **29**: 1499–1504.
8. Choate KA, Khavari PA. Direct cutaneous gene delivery in a human genetic skin disease. *Hum Gene Ther* 1997; **8**: 1659–1665.
9. Temin HM. Safety considerations in somatic gene therapy of human disease with retrovirus vectors. *Hum Gene Ther* 1990; **1**: 111–123.
10. Byrnes AP, Rusby JE, Wood MJ, *et al.* Adenovirus gene transfer causes inflammation in the brain. *Neuroscience* 1995; **66**: 1015–1024.
11. Liu F, Song Y, Liu D. Hydrodynamics-based transfection in animals by systemic administration of plasmid DNA. *Gene Ther* 1999; **6**: 1258–1266.
12. Liu D, Knapp JE. Hydrodynamics-based gene delivery. *Curr Opin Mol Ther* 2001; **3**: 192–197.
13. Herweijer H, Wolff JA. Progress and prospects: naked DNA gene transfer and therapy. *Gene Ther* 2003; **10**: 453–458.
14. Ehrhardt A, Peng PD, Xu H, *et al.* Optimization of cis-acting elements for gene expression from nonviral vectors in vivo. *Hum Gene Ther* 2003; **14**: 215–225.
15. Yant SR, Meuse L, Chiu W, *et al.* Somatic integration and long-term transgene expression in normal and haemophilic mice using a DNA transposon system. *Nat Genet* 2000; **25**: 35–41.
16. Alino SF, Crespo A, Dasi F. Long-term therapeutic levels of human alpha-1 antitrypsin in plasma after hydrodynamic injection of nonviral DNA. *Gene Ther* 2003; **10**: 1672–1679.
17. McCaffrey AP, Meuse L, Pham TT, *et al.* RNA interference in adult mice. *Nature* 2002; **418**: 38–39.
18. Lewis DL, Hagstrom JE, Loomis AG, *et al.* Efficient delivery of siRNA for inhibition of gene expression in postnatal mice. *Nat Genet* 2002; **32**: 107–108.
19. Song E, Lee SK, Wang J, *et al.* RNA interference targeting Fas protects mice from fulminant hepatitis. *Nat Med* 2003; **9**: 347–351.
20. Giladi H, Ketzinel-Gilad M, Rivkin L, *et al.* Small interfering RNA inhibits hepatitis B virus replication in mice. *Mol Ther* 2003; **8**: 769–776.
21. Chang J, Sigal LJ, Lerro A, *et al.* Replication of the human hepatitis delta virus genome Is initiated in mouse hepatocytes following intravenous injection of naked DNA or RNA sequences. *J Virol* 2001; **75**: 3469–3473.
22. Malcolm GN, Rowlinson JS. The thermodynamic properties of aqueous solutions of poly(ethylene glycol), polypropylene glycol and dioxane. *Trans Faraday Soc* 1957; **53**: 921–931.
23. Bessler WG, Schimmelpfeng L, Peters JH. Potentiation of mitogen-induced lymphocyte stimulation by polyethylene glycols. *Biochem Biophys Res Commun* 1977; **76**: 1253–1260.
24. McCammon JR, Fan VS. Release of membrane constituents following polyethylene glycol treatment of HEp-2 cells. *Biochim Biophys Acta* 1979; **551**: 67–73.
25. Boni LT, Hui SW. The mechanism of poly(ethylene glycol)-induced fusion in model membranes. In *Cell Fusion*, Sowers AE (ed). Plenum Press: New York, 1987; 301–330.
26. Herrmann A, Clague MJ, Blumenthal R. Enhancement of viral fusion by nonadsorbing polymers. *Biophys J* 1993; **65**: 528–534.
27. Roos DS, Davidson RL, Choppin PW. Control of membrane fusion in poly(ethylene glycol)-resistant cell mutants: application to fusion technology. In *Cell Fusion*, Sowers AE (ed). Plenum Press: New York, 1987; 123–144.
28. MacDonald RI. Membrane fusion due to dehydration by polyethylene glycol, dextran, or sucrose. *Biochemistry* 1985; **24**: 4058–4066.
29. Burgess SW, McIntosh TJ, Lentz BR. Modulation of poly(ethylene glycol)-induced fusion by membrane hydration: importance of interbilayer separation. *Biochemistry* 1992; **31**: 2653–2661.
30. Ahkong QF, Lucy JA. Osmotic forces in artificially induced cell fusion. *Biochim Biophys Acta* 1986; **858**: 206–216.
31. Zhang G, Gao X, Song YK, *et al.* Hydroporation as the mechanism of hydrodynamic delivery. *Gene Ther* 2004; **11**: 675–682.
32. Nguyen LT, Ishida T, Ukitsu S, *et al.* Culture time-dependent gene expression in isolated primary cultured rat hepatocytes by transfection with the cationic liposomal vector TFL-3. *Biol Pharm Bull* 2003; **26**: 880–885.
33. Tanaka K, Sato M, Tomita Y, *et al.* Biochemical studies on liver functions in primary cultured hepatocytes of adult rats. I. Hormonal effects on cell viability and protein synthesis. *J Biochem (Tokyo)* 1978; **84**: 937–946.
34. Tachibana R, Harashima H, Ide N, *et al.* Quantitative analysis of correlation between number of nuclear plasmids and gene expression activity after transfection with cationic liposomes. *Pharm Res* 2002; **19**: 377–381.

35. Matsuda R, Nishikawa A, Tanaka H. Visualization of dystrophic muscle fibers in mdx mouse by vital staining with Evans blue: evidence of apoptosis in dystrophin-deficient muscle. *J Biochem (Tokyo)* 1995; **118**: 959–964.
36. Price JR. Polyethylene glycol. In *Handbook of Pharmaceutical Excipients*, Wade A, Weller PJ (eds). The Pharmaceutical Press: London, 1994; 355–361.
37. Lemieux P, Guerin N, Paradis G, *et al.* A combination of poloxamers increases gene expression of plasmid DNA in skeletal muscle. *Gene Ther* 2000; **7**: 986–991.
38. Pitard B, Pollard H, Agbulut O, *et al.* A nonionic amphiphile agent promotes gene delivery in vivo to skeletal and cardiac muscles. *Hum Gene Ther* 2002; **13**: 1767–1775.
39. Budker V, Budker T, Zhang G, *et al.* Hypothesis: naked plasmid DNA is taken up by cells in vivo by a receptor-mediated process. *J Gene Med* 2000; **2**: 76–88.
40. Kobayashi N, Kuramoto T, Yamaoka K, *et al.* Hepatic uptake and gene expression mechanisms following intravenous administration of plasmid DNA by conventional and hydrodynamics-based procedures. *J Pharmacol Exp Ther* 2001; **297**: 853–860.
41. Kobayashi N, Nishikawa M, Hirata K, *et al.* Hydrodynamics-based procedure involves transient hyperpermeability in the hepatic cellular membrane: implication of a nonspecific process in efficient intracellular gene delivery. *J Gene Med* 2004; **6**: 584–592.
42. Andrianaivo F, Lecocq M, Wattiaux-De Coninck S, *et al.* Hydrodynamics-based transfection of the liver: entrance into hepatocytes of DNA that causes expression takes place very early after injection. *J Gene Med* 2004; **6**: 877–883.
43. Maeda M, Thompson GA Jr. On the mechanism of rapid plasma membrane and chloroplast envelope expansion in Dunaliella salina exposed to hypoosmotic shock. *J Cell Biol* 1986; **102**: 289–297.
44. Einspahr KJ, Maeda M, Thompson GA Jr. Concurrent changes in Dunaliella salina ultrastructure and membrane phospholipid metabolism after hyperosmotic shock. *J Cell Biol* 1988; **107**: 529–538.
45. Tilly BC, van den Berghe N, Tertoolen LG, *et al.* Protein tyrosine phosphorylation is involved in osmoregulation of ionic conductances. *J Biol Chem* 1993; **268**: 19 919–19 922.
46. Haussinger D, Lang F. Cell volume in the regulation of hepatic function: a mechanism for metabolic control. *Biochim Biophys Acta* 1991; **1071**: 331–350.
47. Poulin R, Pegg AE. Regulation of ornithine decarboxylase expression by anisosmotic shock in alpha-difluoromethylornithine-resistant L1210 cells. *J Biol Chem* 1990; **265**: 4025–4032.
48. Csonka LN. Physiological and genetic responses of bacteria to osmotic stress. *Microbiol Rev* 1989; **53**: 121–147.
49. Brewster JL, de Valoir T, Dwyer ND, *et al.* An osmosensing signal transduction pathway in yeast. *Science* 1993; **259**: 1760–1763.
50. Kabanov AV, Batrakova EV, Sriadibhatla S, *et al.* Polymer genomics: shifting the gene and drug delivery paradigms. *J Control Release* 2005; **101**: 259–271.
51. McNeil PL, Steinhardt RA. Loss, restoration, and maintenance of plasma membrane integrity. *J Cell Biol* 1997; **137**: 1–4.
52. Herweijer H, Zhang G, Subbotin VM, *et al.* Time course of gene expression after plasmid DNA gene transfer to the liver. *J Gene Med* 2001; **3**: 280–291.
53. Miao CH, Ohashi K, Patijn GA, *et al.* Inclusion of the hepatic locus control region, an intron, and untranslated region increases and stabilizes hepatic factor IX gene expression in vivo but not in vitro. *Mol Ther* 2000; **1**: 522–532.

Available online at www.sciencedirect.com
SCIENCE DIRECT®
International Journal of Pharmaceutics 296 (2005) 133–141
international journal of pharmaceutics
www.elsevier.com/locate/ijpharm

Pharmaceutical Nanotechnology

Applicability of anti-neovascular therapy to drug-resistant tumor: Suppression of drug-resistant P388 tumor growth with neovessel-targeted liposomal adriamycin

K. Shimizu[a], T. Asai[a], C. Fuse[a], Y. Sadzuka[b], T. Sonobe[b], K. Ogino[c], T. Taki[c], T. Tanaka[d], N. Oku[a,*]

[a] *Department of Medical Biochemistry and COE Program in the 21st Century, University of Shizuoka School of Pharmaceutical Sciences, 52-1 Yada, Shizuoka 422-8526, Japan*
[b] *Department of Pharmaceutical Engineering, University of Shizuoka School of Pharmaceutical Sciences, 52-1 Yada, Shizuoka 422-8526, Japan*
[c] *Molecular Medical Science Institute, Otsuka Pharmaceutical Co., Ltd., 463-10 Kagasuno, Kawauchi-cho, Tokushima 771-0192, Japan*
[d] *Department of Applied Chemistry, Faculty of Engineering, Nagoya Institute of Technology, Gokiso-cho, Nagoya 466-8555, Japan*

Received 20 December 2004; received in revised form 5 February 2005; accepted 19 February 2005
Available online 11 April 2005

Abstract

Anti-neovascular therapy, one of the effective anti-angiogenic chemotherapy, damages new blood vessels by cytotoxic agents delivered to angiogenic endothelial cells and results in indirect eradication of tumor cells. We previously reported that liposomes-modified with a pentapeptide, Ala-Pro-Arg-Pro-Gly (APRPG-Lip) homing to angiogenic site, highly accumulated in tumor tissue, and APRPG-Lip encapsulating adriamycin (APRPG-LipADM) effectively suppressed tumor growth in tumor-bearing mice. In the present study, we examined the topological distribution of fluorescence-labeled APRPG-LipADM as well as TUNEL-stained cells in an actual tumor specimen obtained from Colon 26 NL-17 carcinoma-bearing mice. The fluorescence-labeled APRPG-Lip dominantly localized to vessel-like structure: A part of which was also stained with anti-CD31 antibody. Furthermore, TUNEL-stained cells were co-localized to the same structure. These data indicated that APRPG-LipADM bound to angiogenic endothelial cells and induced apoptosis of them. We also investigated the applicability of anti-neovascular therapy using APRPG-LipADM to ADM-resistant P388 solid tumor. As a result, APRPG-LipADM significantly suppressed tumor growth in mice bearing the ADM-resistant tumor. These data suggest that APRPG-LipADM is applicable to various kinds of tumor including drug-resistant

Abbreviations: ADM, adriamycin; DSPC, distearoylphosphatidylcholine; FBS, fetal bovine serum; PBS, phosphate-buffered saline; PEG, polyethylene glycol; VEGF, vascular endothelial growth factor

* Corresponding author. Tel.: +81 54 264 5701; fax: +81 54 264 5705.
E-mail address: oku@u-shizuoka-ken.ac.jp (N. Oku).

doi:10.1016/j.ijpharm.2005.02.030

tumor since it targets angiogenic endothelial cells instead of tumor cells, and eradicates tumor cells through damaging the neovessels.

Keywords: Liposome; Anti-neovascular therapy; Angiogenesis; Drug delivery system; Active targeting

1. Introduction

Tumor angiogenesis, construction of new blood vessels in tumor tissue, is critical for tumor growth, since the supply of oxygen and nutrients is essential for many tumors. Angiogenesis is also related to blood-borne metastasis to distal organs, since it is initiated through this angiogenic vasculature (Folkman, 1971). A number of previous studies on angiogenesis have elucidated the functions of pro-angiogenic factors such as vascular endothelial growth factor (VEGF) and the biological process of angiogenesis (Asahara et al., 1999; Ferrara, 2002). Based on these findings, cancer therapy targeted to angiogenesis has been considered and various inhibitors for angiogenic process have been developed (Kerbel and Folkman, 2002). These agents often prevent pro-angiogenic factors from binding to their receptors or inhibit signal transduction in angiogenesis. This therapy is generally called as anti-angiogenic therapy. For example, the treatment of antibody against VEGF receptor, KDR/flk-1 suppressed tumor growth by inhibition of angiogenesis (Brekken et al., 2000). We previously suggested that disruption of angiogenic vasculature by allowing cytotoxic agent to angiogenic endothelial cells could effectively inhibited tumor growth (Oku et al., 2002a). Since angiogenic endothelial cells have acquired enhanced growth ability, cytotoxic anti-cancer agents are able to damage angiogenic endothelial cells as well as tumor cells. This anti-neovascular therapy is expected to overcome several but critical problems in traditional cancer chemotherapy. For example, anti-neovascular therapy can reduce injected dose, since the angiogenic endothelial cells, which should be eradicated by this therapy, are fewer than the tumor cells in a tumor tissue. In addition, this therapy is promising to apply to various kinds of solid tumors including drug-resistant tumors since the nature of angiogenic vessels may be the same or quite similar among tumors despite the tumor cells acquire the drug-resistance (Browder et al., 2000).

In the previous study, we isolated peptides specific for tumor angiogenic vasculature by in vivo biopanning of a phage-displayed peptide library (Oku et al., 2002b). Obtained Ala-Pro-Arg-Pro-Ala (APRPG) peptide was used for an active targeting tool for angiogenic vessels. In fact, APRPG-modified liposomes (APRPG-Lip) highly accumulated in tumor tissue and adriamycin (ADM)-encapsulated APRPG-Lip (APRPG-LipADM) effectively suppressed tumor growth in Meth A sarcoma- and Colon 26 NL-17 carcinoma-bearing model mice. Furthermore, APRPG-Lip bound specifically to VEGF-stimulated human umbilical vein endothelial cells (HUVECs) compared with unmodified ones (Oku et al., 2002b). These findings suggested that APRPG-LipADM shows potent anti-tumor effect in order to eradicate angiogenic vasculature and, therefore, is expected to apply to drug-resistant tumor.

In the present study, to confirm that APRPG-LipADM really damages angiogenic endothelial cells, intratumoral distribution of APRPG-Lip and vessel damage in tumor tissue after the treatment of APRPG-LipADM were examined. Furthermore, to investigate whether APRPG-modified liposomal agent can be applied to drug-resistant cancer, we performed therapeutic experiment using ADM-resistant P388 solid tumor-bearing mice.

2. Materials and methods

2.1. Materials

Stearoyl-APRPG derivative was synthesized as previously described (Asai et al., 2002). Distearoylphosphatidylcholine (DSPC) was a gift from Nippon Fine Chemical Co. Ltd. (Takasago, Hyogo, Japan). Cholesterol was purchased from Sigma Chemical Co. (St. Louis, MO, USA). Balb/c and DBA/2 male mice were purchased from Japan SLC, Inc.

2.2. Liposomal preparation

Liposomal preparation was performed as described previously (Oku et al., 2002b). In brief, DSPC, cholesterol and stearoyl-APRPG derivative (10/5/1 as a molar ratio) dissolved in chloroform were dried under reduced pressure and stored in vacuo for at least 1 h. Constituted lipid thin film was hydrated with 0.3 M citric acid solution (pH 4.0) to generate liposomal solution. This liposomal suspension (10 mM as DSPC) was frozen and thawed for three cycles with liquid nitrogen and sized to 100 nm by extruding through 100 nm-pore sized polycarbonate membrane filter (Advantec, Tokyo, Japan) attached to an extruder (Lipex, Vancouver, BC, Canada). ADM was encapsulated into APRPG-Lip as previously described (Oku et al., 2002b). Particle size of the liposomes was 154 ± 1 nm recorded on an ELS-800 electrophoretic light-scattering spectrophotometer (Otsuka Electronics Co., Ltd., Osaka, Japan), and the liposomes were stable during a 48-h incubation in the presence of 50% fetal bovine serum (FBS, Sigma Chemical Co.) at 37 °C (data not shown). Fluorescence-labeled APRPG-Lip was prepared as follows: Thin film composed of DSPC, cholesterol, and stearoly-APRPG derivative with a trace of $DiIC_{18}$ (Molecular Probes Inc., Eugene, OR, USA) was hydrated with 0.3 M glucose solution (DSPC/cholesterol/stearoyl APRPG derivative/$DiIC_{18}$ = 10/5/1/0.1 as a molar ratio, 10 mM as DSPC). Obtained liposomal suspension was extruded with a 100 nm-pored filter.

2.3. Preparation of tumor-bearing mice

Mouse Colon 26 NL-17 carcinoma (C26 NL-17) cells were grown in RPMI 1640 with 10% FBS at 37 °C in the presence of 5% CO_2. P388 and P388/ADM leukemia cells were grown in abdominal cavity of DBA/2 mouse. C26 NL-17, P388 or P388/ADM cells (1×10^6 cells per mouse) were subcutaneously implanted into left posterior flank of Balb/c male mice for C26 NL-17 or DBA/2 male mice for P388 and P388/ADM, respectively.

2.4. Intratumoral distribution of liposomes

$DiIC_{18}$-labeled APRPG-Lip or $DiIC_{18}$-labeled unmodified liposome (Cont-Lip) were administered via a tail vein of C26 NL-17-bearing mice when the tumor sizes had reached about 1 cm in diameter. Fifteen minutes or 2 h after injection of liposomes, mice were sacrificed under anesthesia with diethyl ether and tumors were dissected and kept in 20% formalin. Solid tumors were wrapped in O.C.T. compound (Sakura Finetechnochemical Co. Ltd., Tokyo, Japan) and frozen at −80 °C. Five-micrometer tumor sections were prepared by using cryostatic microtome (HM 505E, Microm, Walldorf, Germany). For endothelial cell staining, sections were washed and incubated with biotinylated anti-mouse CD31 antibody (PharMingen, San Diego, CA, USA) in wet chamber at room temperature, after the sections had been blocked with 1% BSA–PBS (−). After 1-h incubation, sections were washed and secondly stained with streptavidin–FITC conjugate (Molecular Probes Inc., Eugene, OR, USA) for 30 min. These sections were fluorescently observed by using microscopic LSM system (Carl Zeiss, Co. Ltd.).

2.5. Determination of apoptotic cells in tumor

ADM-encapsulated Cont-Lip (Cont-LipADM) or APRPG-LipADM (10 mg/kg as dose of ADM) were administered via a tail vain of C26 NL-17-bearing mice or P388/ADM-bearing mice when the tumor sizes had reached about 1 cm in diameter for C26 NL-17-bearing mice and at day 6 for P388/ADM-bearing mice, respectively. Two days after injection of liposomal ADM, each solid tumor was dissected from the mice and tumor sections were prepared as described in Section 2.4. Immunostaining of endothelial cells was performed as described in Section 2.4, except that streptavidin–Alexa 594 conjugate (Molecular Probes Inc., Eugene, OR, USA) was used as fluorescent dye instead of streptavidin–FITC conjugate. For visualizing apoptotic cells, TUNEL staining was performed by use of ApopTag Plus Fluorescein In Situ Apoptosis Detection Kit (Intergen Co., Purchase, NY, USA) according to the recommended procedures of the Kit. In brief, tumor sections were washed and equilibrated for 15 min in wet chamber at room temperature, and sections were reacted with TdT enzyme for 1 h at 37 °C. Then, sections were stained with anti-digoxigenin–fluorescein antibody. These sections were observed with LSM system.

In some experiments, fixed tumor sections were stained with hematoxylin and eosin. In brief, sections were stained with Lillie-Mayer's hematoxylin (Muto

Pure Chemicals. Ltd., Tokyo, Japan) for 2 min and subsequently adjusted the color shade by 50 mM Tris-buffered saline, pH 7.5. Then, the sections were stained with eosin Y (Wako Chemical Co., Osaka, Japan) for 30 s and dehydrated with ethanol. The sections were mounted with DIATEX (AB Wilh. Becker, Stockholm, Sweden) and observed by light microscopy (Olympus, Tokyo, Japan).

2.6. Therapeutic experiment

Cont-LipADM or APRPG-LipADM were intravenously administered (10 mg/kg as dose of ADM) via a tail vein into P388- or P388/ADM-bearing mice at day 6 after tumor implantation. Tumor sizes were examined at selected days after the treatment and the tumor volume was calculated in an established formula 0.4 ($a \times b^2$), where 'a' was the largest and 'b' was the smallest diameter of the tumor. Body weight of each mouse was also monitored after injection of the formulations to evaluate the side effect.

2.7. Statistical analysis

Variance in a group was evaluated by the F-test, and differences in mean tumor volume were evaluated by Student's t-test.

3. Results

3.1. Intratumoral distribution of APRPG-Lip

Previous study showed that APRPG-Lip highly accumulated in tumor tissue in vivo and bound to VEGF-stimulated human endothelial cells in vitro (Oku et al., 2002b), although the actual binding of APRPG-Lip to tumor angiogenic vasculature has not been determined. Therefore, we examined the intratumoral distribution of APRPG-Lip by confocal laser scanning microscopy. Fluorescently labeled APRPG-Lip or Cont-Lip was administered intravenously into C26 NL-17-bearing mice and allowed to circulate for 15 min or 2 h. The tumor was dissected, devoted to immunofluorescence staining of endothelial cells, and examined liposomal distribution. Fluorescence micrographs 2 h after injection of the liposomes are shown in Fig. 1. As shown in the figure, fluorescence of APRPG-Lip was dominantly observed as vessel like structure and some of fluorescent dots were co-localized with CD31 staining (Fig. 1c and d). In contrast, fluorescence of Cont-Lip was observed in all over the tumor tissue without co-localization with CD31 (Fig. 1b). Similar results were also observed 15 min after injection (data not shown). These data suggest that APRPG-Lip bound to tumor angiogenic endothelial cells in an actual tumor tissue.

3.2. Apoptosis of angiogenic endothelial cells by APRPG-LipADM

Since APRPG-Lip seemed specifically bound to angiogenic endothelial cells in tumor tissue, it is possible that APRPG-LipADM damages the cells. Therefore, we determined the apoptotic cells in tumor tissue after treatment of APRPG-LipADM by using double immunostaining method, namely, CD31 staining for observing endothelial cells and TUNEL staining for observing apoptotic cells. Cont-LipADM

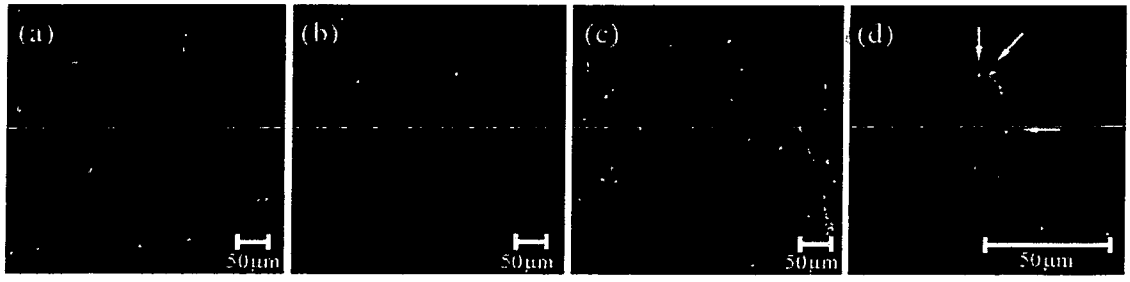

Fig. 1. Binding of APRPG-Lip to tumor angiogenic endothelial cells. C26 NL-17-bearing mice were intravenously administered with glucose (a), DiI-labeled Cont-Lip (b) or DiI-labeled APRPG-Lip (c) on day 17 after tumor implantation. Two hours later, each tumor was dissected, prepared for frozen-section and devoted to CD31-immunostaining to stain endothelial cells (green). Panel (d) shows the magnified image of the area of interest in panel (c). Liposomal fluorescence is shown in red. White arrows show the co-localization of liposomes with the marker of endothelial cells.

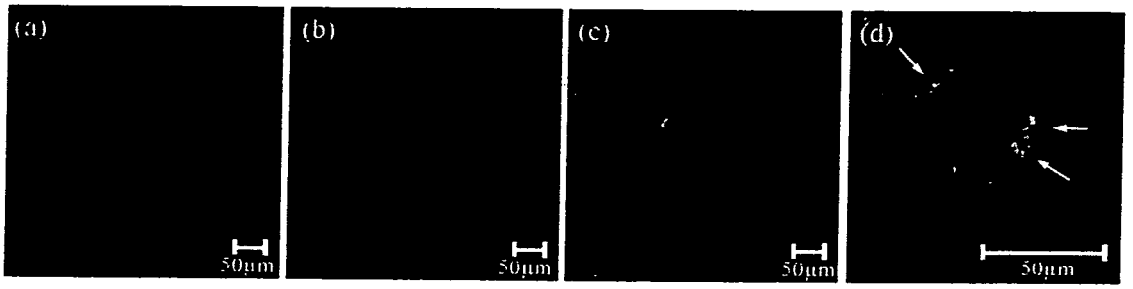

Fig. 2. Double immunostaining of endothelial cells and apoptotic cells on C26 NL-17 tumor following the treatment of APRPG-LipADM. C26 NL-17-bearing mice were administered with glucose (a), Cont-LipADM (b) or APRPG-LipADM (c) (10 mg/kg as dose of ADM) on day 19 after tumor implantation. Two days later, each tumor was dissected and prepared for frozen-section. Microvessels were stained with red (CD31-staining) and apoptotic cells were stained with green (TUNEL method). Panel (d) shows the magnified image of the area of interest in panel (c). White arrows showed apoptotic endothelial cells (yellow).

or APRPG-LipADM was intravenously administered into C26 NL-17-bearing mice, and tumor was dissected, sectioned at 5 μm, and stained at 48 h after the administration. Each derived section was fluorescently observed by use of confocal laser scanning microscopy. As a result, the apoptotic cells located widespread in the tumor and some of them located on the vessel like structure after the treatment of APRPG-LipADM (Fig. 2c and d). Furthermore, CD31 staining was observed on the same vessel like structure. These data strongly suggested that APRPG-LipADM induced apoptosis of both angiogenic endothelial cells and surrounding tumor cells in the solid tumor. In contrast, apoptotic cells located apart from each other, and none of them was co-localized with CD31 staining after the treatment of Cont-LipADM (Fig. 2b).

3.3. Therapeutic experiment using APRPG-LipADM against ADM-resistant tumor

Next, we performed therapeutic experiment using APRPG-LipADM against ADM-resistant tumor. Free ADM, Cont-LipADM or APRPG-LipADM was administered into drug-sensitive P388- or P388/ADM-bearing mice and the tumor regression was evaluated. When we examined the anti-tumor effect against ADM-sensitive P388-bearing mice, free ADM and Cont-LipADM as well as APRPG-LipADM suppressed tumor growth (Fig. 3a). In contrast, treatment of free ADM or Cont-LipADM rarely showed the suppression of tumor growth of P388/ADM-bearing mice under the present experimental condition (Fig. 3b). On the contrary, APRPG-LipADM significantly suppressed tumor growth of P388/ADM solid tumor under the present experimental condition that free ADM or Cont-LipADM did not show the therapeutic effect (Fig. 3b). These data suggest that APRPG-LipADM is superior to free ADM or Cont-LipADM for the treatment of ADM-resistant tumor. Moreover, APRPG-LipADM, as well as Cont-LipADM, did not show the body weight loss, an indicator for side effects, unlike free ADM administration (data not shown).

To confirm the possibility that APRPG-LipADM suppressed tumor growth through damaging angiogenic endothelial cells of ADM-resistant tumor, we performed double immunostaining of apoptotic cells and endothelial cells on tumor section treated with Cont-LipADM or APRPG-LipADM. As shown in Fig. 4, a few apoptotic cells apart from each other was observed after the treatment of Cont-LipADM, and lining apoptotic cells co-localized with CD31 staining was observed after the treatment with APRPG-LipADM. In the case of APRPG-LipADM treatment, many apoptotic cells were also observed around the lining apoptotic cells. These data suggest that APRPG-LipADM induced apoptosis of endothelial cells which caused surrounding tumor cell apoptosis due to cut off of oxygen and nutrients through damaging the neovessels. Hematoxylin and eosin stained tumor sections also indicate that the number of vessel like structures was reduced after the treatment with APRPG-LipADM (Fig. 4, upper right). These data suggest that APRPG-LipADM suppressed drug-resistant tumor growth through the eradication of angiogenic endothelial cells and subsequent disruption of angiogenic vasculature.

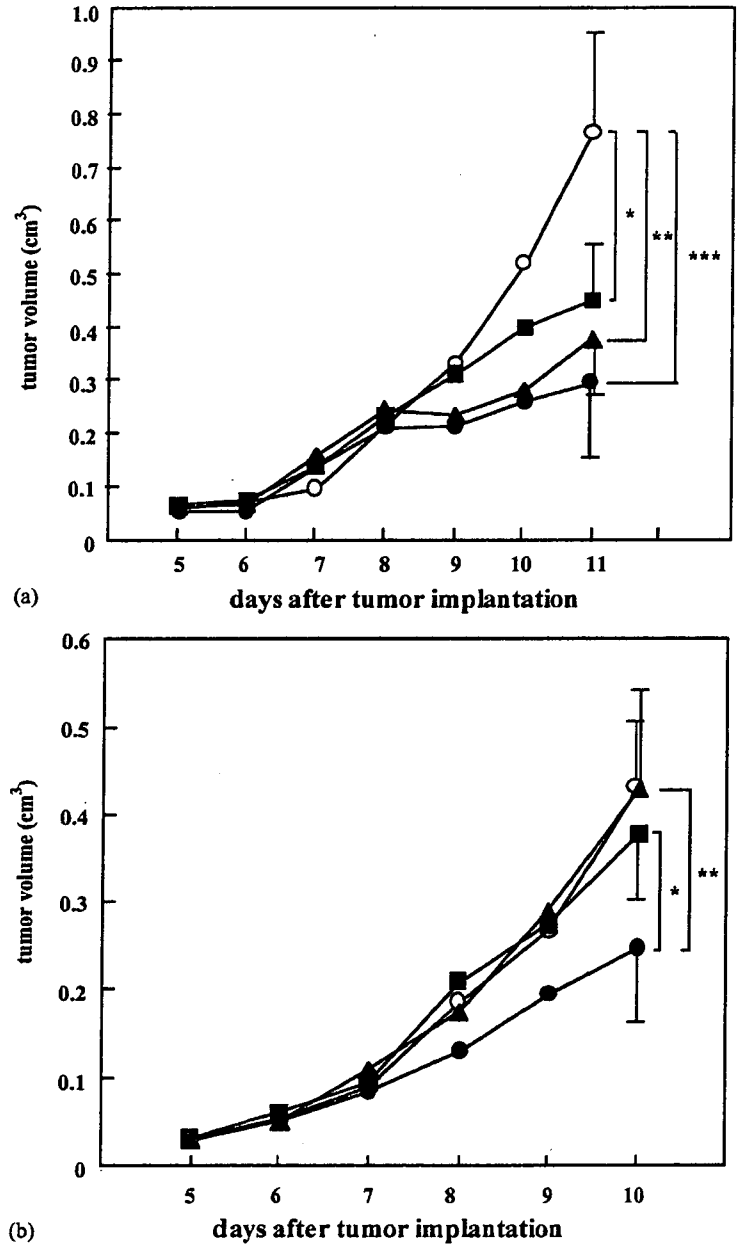

Fig. 3. Suppression of tumor growth by APRPG-LipADM in ADM-resistant tumor-bearing mice. The mice bearing P388 (a) or P388/ADM (b) ($n=5$) were intravenously administered with glucose (○), free ADM (■), Cont-LipADM (▲), or APRPG-LipADM (●) (10 mg/kg as dose of ADM) at day 6 after tumor implantation. Evaluation of tumor regression was described in Section 2. Data points represent the mean ± S.D.; and S.D. bars are shown only for the data points of day 11 for (a) and day 10 for (b), respectively, for the sake of graphic clarity. Significant difference from control (a) or from APRPG-LipADM treatment (b) is shown ($^{*}P<0.05$; $^{**}P<0.01$; $^{***}P<0.001$).

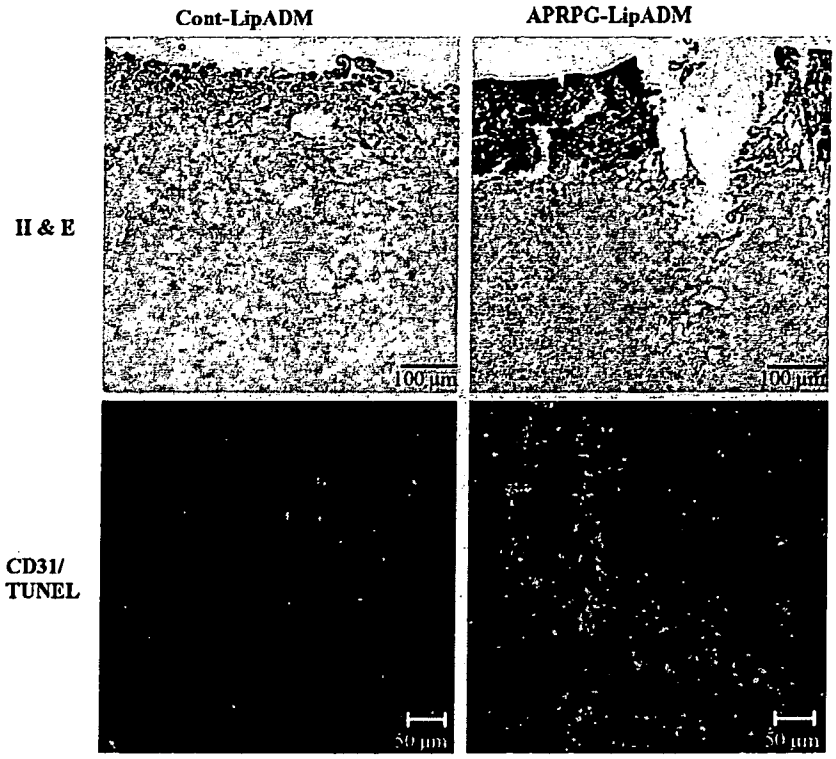

Fig. 4. Histological and immunochemical analysis of ADM-resistant tumor treated with APRPG-LipADM. Tumor sections were prepared as described in Section 2. Upper panels show the micrographs of tumor section stained with hematoxylin–eosin. In histological analysis, edges of tumor sections were observed. Lower panels show the fluorescence micrographs of tumor section immunostained with CD-31 (red) and TUNEL-stained (green). Yellow shows the apoptotic endothelial cells.

4. Discussion

Cytotoxic agents against rapidly growing cells are commonly used for cancer chemotherapy. These agents effectively eradicate cancerous cells, but also damage rapidly dividing normal cells such as bone marrow cells and intestinal lining cells. This is the most serious problem as severe side effects in traditional cancer chemotherapy. Additionally, tumor cells tend to acquire the drug resistance because of their gene instability (Bailar and Gornik, 1997), and therefore a certain cytotoxic agent at selected dose cannot affect on tumor cells. These problems further burden the patients on therapeutic treatment. For these reasons, the development of strategies for cancer chemotherapy such as usage of DDS technology has been required.

Since Folkman et al. advocates the necessity of angiogenesis in tumor progression (Folkman, 1971), a novel strategy for cancer therapy, which is called anti-angiogenic therapy, has been focused and various kinds of angiogenic inhibitor has been developed (Kerbel and Folkman, 2002). There may be some advantages of anti-angiogenic therapy over traditional cancer therapy: Anti-angiogenic therapy can reduce the side effects due to appreciable specificity to angiogenic endothelial cells (Brooks et al., 1994, 1996) and due to reduction of injected dose since angiogenic endothelial cells account for low population compared with tumor cells in tumor tissue. Anti-angiogenic therapy can get rid of concern about acquirement of drug-resistance because this therapy targets normal endothelial cells. Anti-angiogenic therapy may be applicable to most kinds of tumor including drug-resistant tumor because they often induce similar angiogenesis despite of them for their maintenance and development.

Recently, we developed a novel anti-angiogenic therapy, anti-neovascular therapy (Oku et al., 2002a). The concept of this therapy is different from conven-

tional anti-angiogenic therapy in that anti-neovascular therapy does not inhibit a part of angiogenic process but directly eradicate angiogenic endothelial cells by using DDS drugs against neovessels (Shimizu and Oku, 2004). As a result, this therapy strongly promises disruption of angiogenic vasculature following effective suppression of tumor growth with little side effects. To develop an angiogenic vasculature-targeting carrier for cytotoxic agents, we firstly determined pentapeptide sequence (APRPG), which had high affinity to angiogenic site. Cytotoxic agents-encapsulating liposomes modified with the peptide showed enhanced anti-tumor effect (Oku et al., 2002b; Asai et al., 2002).

We hypothesized that APRPG-LipADM caused tumor regression through damaging the neovessels. In the present study, we firstly investigated the intratumoral distribution of APRPG-LipADM and topological distribution of apoptotic cells after the treatment with APRPG-LipADM. The specific binding of APRPG-Lip to angiogenic endothelial cells in tumor tissue was observed (Fig. 1c and d), suggesting that APRPG-Lip actively targets and binds to angiogenic endothelial cells in tumor tissue after intravenous administration. Moreover, the data of Fig. 2 suggested that APRPG-LipADM induced apoptosis of endothelial cells as well as tumor cells in tumor tissue. In contrast, Cont-LipADM seemed to damage only tumor cells. We speculate that APRPG-LipADM directly eradicate angiogenic endothelial cells. Although it is still ambiguous whether tumor cells are directly damaged by APRPG-LipADM or their apoptosis is caused by cut off of oxygen and nutrients through damaging the endothelial cells. Even if, both mechanisms might be worked, we speculate that the latter contribute more than the former, since angiogenic vessels might be damaged by APRPG-LipADM, and since the population of apoptotic cells in tumor tissues is greater for APRPG-LipADM-treated group than for Cont-LipADM-treated one.

If the majority of tumor cells are damaged indirectly through the damage of neovessels after treatment with APRPG-LipADM, this formulation of ADM may also cause damage of ADM-resistant tumor. Therefore, we challenged to apply the APRPG-LipADM against ADM-resistant tumor. As a result, APRPG-LipADM actually suppressed tumor growth (Fig. 3). Since a single dose of treatment of free ADM or Cont-LipADM was not toxic to ADM-resistant tumor cells whereas they suppressed tumor growth of ADM-sensitive tumor cells, APRPG-LipADM may damage growing angiogenic endothelial cells, which causes the suppression for tumor growth indirectly. In fact, we observed the apoptotic cells in angiogenic vessels and in surrounding tumor tissue of ADM-resistant tumor after the treatment of APRPG-LipADM, (Fig. 4). These results indicate that APRPG-LipADM actively disrupts angiogenic vasculature and subsequently suppresses the ADM-resistant tumor growth. The present study strongly suggests that APRPG-LipADM targets to angiogenic vasculature and has potent anti-tumor effect against various kinds of tumor including drug-resistant tumor. Furthermore, reduction of severe side effects is expected by use of APRPG-LipADM due to targeting effects. The modification of liposomes with hexapeptide, GPLPLR, targeted to membrane-type 1 matrix metalloproteinase (MT1-MMP), which is expressed on the surface of angiogenic endothelial cells, also enhanced anti-tumor activity of encapsulated hydrophobic anti-cancer drug (Kondo et al., 2004).

Recently, we observed that APRPG-polyethyleneglycol (PEG) modified liposomes (APRPG-PEG-Lip) showed long-circulating character and accumulated in tumor tissue of tumor-bearing mice (Maeda et al., 2004a). Administration of these liposomes encapsulating ADM into tumor-bearing mice caused strong suppression of tumor growth without remarkable side effects (Maeda et al., 2004b). Availability of anti-neovascular therapy by using PEG-coated angiogenic-vasculature targeting liposomal agent was also reported by several research groups: One used NGR peptide as a targeting probe (Pastorino et al., 2003), and another used RGD peptide (Schiffelers et al., 2003). These accumulating data from ours and other research groups indicate the usefulness of anti-neovascular therapy using DDS drugs in the treatment of cancer, and the present study additionally confirms the availability of the therapy for drug-resistance-acquired cancer.

Acknowledgements

Authors thank Mr. S. Tajima for the technical assistance. This work was supported in part by a Grant-in-Aid for Scientific Research from the Japan Society for the Promotion of Science.

References

Asahara, T., Takahashi, T., Masuda, H., Kalka, C., Chen, D., Iwaguro, H., Inai, Y., Silver, M., Isner, J.M., 1999. VEGF contributes to postnatal neovascularization by mobilizing bone marrow-derived endothelial progenitor cells. EMBO J. 18, 3964–3972.

Asai, T., Shimizu, K., Kondo, M., Kuromi, K., Watanabe, K., Ogino, K., Taki, T., Shuto, S., Matsuda, A., Oku, N., 2002. Anti-neovascular therapy by liposomal DPP-CNDAC targeted to angiogenic vessels. FEBS Lett. 520, 167–170.

Bailar 3rd, J.C., Gornik, H.L., 1997. Cancer undefeated. N. Engl. J. Med. 336, 1569–1574.

Brekken, R.A., Overholser, J.P., Stastny, V.A., Waltenberger, J., Minna, J.D., Thorpe, P.E., 2000. Selective inhibition of vascular endothelial growth factor (VEGF) receptor 2 (KDR/Flk-1) activity by a monoclonal anti-VEGF antibody blocks tumor growth in mice. Cancer Res. 60, 5117–5124.

Brooks, P.C., Clark, R.A., Cheresh, D.A., 1994. Requirement of vascular integrin alpha v beta 3 for angiogenesis. Science 264, 569–571.

Brooks, P.C., Stromblad, S., Sanders, L.C., von Schalscha, T.L., Aimes, R.T., Stetler-Stevenson, W.G., Quigley, J.P., Cheresh, D.A., 1996. Localization of matrix metalloproteinase MMP-2 to the surface of invasive cells by interaction with integrin alpha v beta 3. Cell 85, 683–693.

Browder, T., Butterfield, C.E., Kraling, B.M., Shi, B., Marshall, B., O'Reilly, M.S., Folkman, J., 2000. Antiangiogenic scheduling of chemotherapy improves efficacy against experimental drug-resistant cancer. Cancer Res. 60, 1878–1886.

Ferrara, N., 2002. VEGF and the quest for tumour angiogenesis factors. Nat. Rev. Cancer 2, 795–803.

Folkman, J., 1971. Tumor angiogenesis: therapeutic implications. N. Engl. J. Med. 285, 1182–1186.

Kerbel, R., Folkman, J., 2002. Clinical translation of angiogenesis inhibitors. Nat. Rev. Cancer 2, 727–739.

Kondo, M., Asai, T., Katanasaka, Y., Sadzuka, Y., Tsukada, H., Ogino, K., Taki, T., Baba, K., Oku, N., 2004. Anti-neovascular therapy by liposomal drug targeted to membrane type-1 matrix metalloproteinase. Int. J. Cancer 108, 301–306.

Maeda, N., Takeuchi, Y., Takada, M., Namba, Y., Oku, N., 2004a. Synthesis of angiogenesis-targeted peptide and hydrophobized polyethylene glycol conjugate. Bioorg. Med. Chem. Lett. 14, 1015–1017.

Maeda, N., Takeuchi, Y., Takada, M., Sadzuka, Y., Namba, Y., Oku, N., 2004b. Anti-neovascular therapy by use of tumor neovasculature-targeted long-circulating liposome. J. Controlled Release 100, 41–52.

Oku, N., Asai, T., Kurohane, K., Watanabe, K., Kuromi, K., Namba, Y., Ogino, K., Taki, T., 2002a. Cancer antineovascular therapy. Cell. Mol. Biol. Lett. 7, 247–248.

Oku, N., Asai, T., Watanabe, K., Kuromi, K., Nagatsuka, M., Kurohane, K., Kikkawa, H., Ogino, K., Tanaka, M., Ishikawa, D., Tsukada, H., Momose, M., Nakayama, J., Taki, T., 2002b. Anti-neovascular therapy using novel peptides homing to angiogenic vessels. Oncogene 21, 2662–2669.

Pastorino, F., Brignole, C., Marimpietri, D., Cilli, M., Gambini, C., Ribatti, D., Longhi, R., Allen, T.M., Corti, A., Ponzoni, M., 2003. Vascular damage and anti-angiogenic effects of tumor vessel-targeted liposomal chemotherapy. Cancer Res. 63, 7400–7409.

Schiffelers, R.M., Koning, G.A., ten Hagen, T.L., Fens, M.H., Schraa, A.J., Janssen, A.P., Kok, R.J., Molema, G., Storm, G., 2003. Anti-tumor efficacy of tumor vasculature-targeted liposomal doxorubicin. J. Controlled Release 91, 115–122.

Shimizu, K., Oku, N., 2004. Cancer anti-angiogenic therapy. Biol. Pharm. Bull. 27, 599–605.

Available online at www.sciencedirect.com
SCIENCE DIRECT
Biochimica et Biophysica Acta 1669 (2005) 69–74
BIOCHIMICA ET BIOPHYSICA ACTA
BBA
http://www.elsevier.com/locate/bba

Antiangiogenic photodynamic therapy (PDT) by using long-circulating liposomes modified with peptide specific to angiogenic vessels

Kanae Ichikawa[a], Tomoya Hikita[a], Noriyuki Maeda[a,b], Sei Yonezawa[a], Yoshito Takeuchi[a], Tomohiro Asai[a], Yukihiro Namba[b], Naoto Oku[a,*]

[a]*Department of Medical Biochemistry and COE Program in the 21st Century, University of Shizuoka School of Pharmaceutical Sciences, 52-1 Yada, Shizuoka 422-8526, Japan*
[b]*Nippon Fine Chemical Co. Ltd., Takasago, Hyogo 676-0074, Japan*

Received 23 August 2004; received in revised form 2 February 2005; accepted 2 February 2005
Available online 16 March 2005

Abstract

For the improvement of therapeutic efficacy in photodynamic therapy (PDT) by using a photosensitizer, benzoporphyrin derivative monoacid ring A (BPD-MA), we previously prepared polyethylene glycol (PEG)-modified liposomes encapsulating BPD-MA (PEG-Lip BPD-MA). PEGylation of liposomes enhanced the accumulation of BPD-MA in tumor tissue at 3 h after injection of it into Meth-A-sarcoma-bearing mice, but, unexpectedly, decreased the suitability of the drug for PDT when laser irradiation was performed at 3 h after the injection of the liposomal photosensitizer. To improve the bioavailability of PEG-Lip BPD-MA, we endowed the liposomes with active-targeting characteristics by using Ala-Pro-Arg-Pro-Gly (APRPG) pentapeptide, which had earlier been isolated as a peptide specific to angiogenic endothelial cells. APRPG-PEG-modified liposomal BPD-MA (APRPG-PEG-Lip BPD-MA) accumulated in tumor tissue similarly as PEG-Lip BPD-MA and to an approx. 4-fold higher degree than BPD-MA delivered with non-modified liposomes at 3 h after the injection of the drugs into tumor-bearing mice. On the contrary, unlike the treatment with PEG-Lip BPD-MA, APRPG-PEG-Lip BPD-MA treatment strongly suppressed tumor growth after laser irradiation at 3 h after injection. Finally, we observed vasculature damage in the dorsal air sac angiogenesis model by APRPG-PEG-Lip BPD-MA-mediated PDT. The present results suggest that antiangiogenic PDT is an efficient modality for tumor treatment and that tumor neovessel-targeted, long-circulating liposomes are a useful carrier for delivering photosensitizer to angiogenic endothelial cells.

Keywords: Photodynamic therapy (PDT); Targeting; Polyethylene glycol (PEG); Liposome; Angiogenesis

1. Introduction

Angiogenesis is a crucial event for solid tumor growth, since the tumor cells demand oxygen and nutrients. Therefore, the suppression of angiogenesis is expected to show potent therapeutic effects on various cancers [1,2]. Moreover, antiangiogenic therapy is thought not only to eradicate primary tumor cells, but also to suppress hematogenous metastasis through the disruption of the metastatic pathway. Recent studies also indicate the usefulness of antiangiogenic photodynamic therapy (PDT) [3,4]. Photodynamic therapy (PDT) is a promising modality for cancer treatment that uses a combination of photosensitizer and tissue-penetrating laser light without severe side effects [5]. After laser irradiation, singlet oxygen is produced by the photosensitizer and induces cytotoxicity. In this study, we used a second-generation photosensitizer, benzoporphyrin derivative monoacid ring A (BPD-MA), which required liposomalization due to its hydrophobic property.

In a previous study, we established a rather stable liposomal BPD-MA (dipalmitoylphosphatidylcholine [DPPC]/palmitoyloleoylphosphatidylcholine [POPC]/cholesterol/dipalmitoylphosphatidylglycerol [DPPG]/BPD-MA=10/10/10/2.5/0.3 as molar ratio) [6]. Antiangiogenic

* Corresponding author.
E-mail address: oku@u-shizuoka-ken.ac.jp (N. Oku).

0005-2736/$ - see front matter © 2005 Elsevier B.V. All rights reserved.
doi:10.1016/j.bbamem.2005.02.003

PDT, i.e., laser irradiation at 15 min after the injection of the liposomal BPD-MA, suppressed tumor growth more efficiently than conventional PDT did, i.e., laser irradiation at 3 h post injection. This scheduling of PDT caused hemostasis due to damaged angiogenic endothelial cells [7]. Although in clinical usage, 3-h PDT has been traditionally performed, since the concentration of BPD-MA in tumor tissue is higher than in normal tissue at 3 h after the injection. Furthermore, because the photosensitizer is distributed in the plasma at 15 min after the injection, antiangiogenic PDT may damage the blood cells more than would conventional PDT scheduling.

For the purpose of enhancing the therapeutic efficacy of liposomal BPD-MA in the conventional scheduling of PDT, we previously prepared polyethylene glycol (PEG)-coated-liposomal BPD-MA, since the long-circulating characteristic of liposomes achieved by PEG-coating is known to bring passive accumulation of liposomal drugs in tumor tissues of tumor-bearing animals [8]. In this case, we aimed at damaging tumor cells rather than angiogenic endothelial cells. However, the therapeutic efficacy after PDT was unexpectedly decreased by the PEG-modification [9]. The PEGylation of liposomes actually enhanced the passive accumulation of the liposomal drug in tumor tissues at 3 h after administration, but did not enhance the therapeutic efficacy after PDT. We speculate the reason to be that the PEG-liposomal BPD-MA (PEG-Lip BPD-MA) was not taken up effectively into the tumor cells before the laser irradiation at 3 h after administration of PEG-Lip BPD-MA. The active oxygen generated by laser irradiation in the PEG liposomes, which resided in the interstitial space of the tumor tissue, might not have damaged the cells around the liposomes, since the half-life of active oxygen is too short for the radical to pass from the inside of the liposomes to the cells.

On the other hand, for the purpose of antineovascular therapy (ANET), we previously used in vivo biopanning of a phage-displayed peptide library to isolate a 5-mer peptide, Ala-Pro-Arg-Pro-Gly (APRPG), that specifically bound to the tumor angiogenic site [10,11]: The accumulation of APRPG-presenting phages in the tumor tissue was specifically inhibited in the presence of APRPG-containing peptide, and APRPG-containing peptide was specifically bound to angiogenic endothelial cells determined by histochemical studies [10]. The APRPG peptide thus obtained was used for the modification of the liposomes; and these liposomes accumulated highly in tumor tissue and adriamycin-encapsulated APRPG-modified liposomes effectively suppressed tumor growth in Meth-A sarcoma- and Colon 26 NL-17 carcinoma-bearing model mice. Furthermore, the PEG-modification of APRPG-liposomes (APRPG-PEG-Lip) prepared with APRPG-PEG-distearoylphosphatidylethanolamine showed enhanced accumulation in Colon 26 NL-17 carcinoma-bearing mice; and adriamycin-encapsulated APRPG-PEG-Lip suppressed tumor growth notably [12].

In the present study, because non-targeting PEG-Lip BPD-MA did not have any drastic effect on tumor growth after the PDT treatment, we examined the applicability of APRPG-PEG-Lip to PDT, since active-targeting liposomes would be expected to bind to and to be taken up effectively by the target cells and damage them. Furthermore, pronounced PDT efficacy would be expected for active-targeting to angiogenic endothelial cells, since antiangiogenic scheduling of PDT is far more effective than conventional scheduling and active-targeting should enable antiangiogenic PDT despite the later time of irradiation. Therefore, in the present study, we examined tumor growth suppression after 3-h PDT by using APRPG-PEG-Lip BPD-MA, which is actively targeted to angiogenic endothelial cells in comparison with PEG-Lip BPD-MA, which is passively targeted to tumor tissue.

2. Materials and methods

2.1. Materials

DPPC, POPC, DPPG, and PEG-DSPE were the products of Nippon Fine Chemical Co., Ltd (Takasago, Hyogo, Japan). Cholesterol was purchased from Sigma Chemical Co. (St Louis, MO, USA). APRPG-PEG-DSPE was synthesized as described previously [13]. BPD-MA was kindly donated by QLT Photo Therapeutics, Inc. (Vancouver, British Columbia, Canada).

2.2. Preparation and characterization of BPD-MA liposomes

DPPC, POPC, cholesterol, DPPG, and BPD-MA (10/10/10/2.5/0.3 as a molar ratio) without or with PEG-DSPE or APRPG-PEG-DSPE (Lipids/PEG-DSPE or APRPG-PEG-DSPE=20/1) dissolved in chloroform were evaporated, dried under reduced pressure, and stored in vacuo for at least 1 h. The thin lipid film was hydrated with saline and frozen-and-thawed for 3 cycles by using liquid nitrogen. Then the liposomal suspension was sonicated for 15 min at 60 °C. Finally, the liposomes were sized at a 100-nm diameter by extrusion through a polycarbonate membrane filter. The particle sizes and ζ-potential of the liposomes encapsulating BPD-MA were determined by use of an ELS-800 electrophoretic light-scattering spectrophotometer (Otsuka Electronics Co., Ltd., Osaka, Japan). Liposomal aggregation in the presence of serum was determined as follows: Liposomes prepared in 0.3 M glucose were incubated in saline or in 50% FBS for 60 min at 37 °C (final concentration of liposomes was 0.5 mM as PC). The turbidity of the liposomal solution was determined at 750 nm.

The quantification of BPD-MA was performed as follows: A liposomal solution was diluted appropriately with phosphate-buffered saline (PBS, pH 7.4) and mixed

with 3 volumes of MeOH, followed by 1 volume of $CHCl_3$. The absorbance at 688 nm was then determined, and the amount of BPD-MA was calculated from the standard curve.

2.3. Biodistribution of liposomal BPD-MA in tumor tissue assessed by HPLC

Seven days after the implantation of Meth-A sarcoma cells (1×10^6 cells/0.2 mL) into the left posterior flank of 5-week-old male BALB/c mice (Japan SLC, Shizuoka, Japan), the tumor-bearing mice were injected intravenously with liposomal BPD-MA (2 mg/kg as BPD-MA). The mice were sacrificed at 3 h post injection under anesthesia with diethyl ether, and the tumor was excised from each mouse and homogenized in acetate-buffered saline, pH 5.0. Then, BPD-MA was extracted with ethyl acetate thrice. After the evaporation of the solvent, the sample was completely dried in vacuo for overnight and BPD-MA was resolved in DMSO. The amount of BPD-MA was analyzed with HPLC (Shimazu, Japan) equipped with an ultraspere C-8 column (Beckman). The mobile phase for the HPLC analysis was composed of 0.08 M $(NH_4)_2SO_4$, acetonitrile, tetrahydrofuran, and acetic acid (52:28:28:5).

2.4. Antitumor activity in vivo

Meth-A sarcoma-bearing mice (n=9 or 10) were injected intravenously with liposomal BPD-MA (0.5 mg/kg as BPD-MA) at day 7 after tumor implantation. Then the tumor site was irradiated with 689 nm laser light (150 J/cm^2, 0.25 W) at 3 h post-injection. The control group was injected intravenously with saline without laser irradiation. The size of the tumor and body weight of each mouse were monitored thereafter. Two bisecting diameters of each tumor were measured with slide calipers to determine the tumor volume; and calculation was performed by using the formula $0.4(a\times b^2)$, where a is the largest, and b, the smallest, diameter. The tumor volume thus calculated correlated well with the actual tumor weight (r=0.980). The animals were cared for according to the Guidelines for the Care and Use of Laboratory Animals of the University of Shizuoka.

2.5. Preparation of dorsal air sac-model mice

All instruments for preparation of the dorsal air sac were obtained from Millipore Corporation (Bedford, MA, USA). Meth-A sarcoma cells (1×10^7 cells/0.15 mL) were loaded into a Millipore chamber ring covered with Millipore filters having a 0.45-μm pore size. The chamber ring was then implanted s.c. into the dorsum of each of 12 BALB/c mice (5-week-old, male) under pentobarbital anesthesia. At day 4 after the implantation of the chamber ring, PDT treatment was performed by an i.v. injection of liposomal BPD-MA (0.5 mg/kg) followed by exposure to a laser light of 689 nm with 150 J/cm^2 of fluence 3 h post injection. At 24 h after laser irradiation, the mice were sacrificed with diethylether and the dorsal skin that had osculated the chamber ring was observed.

2.6. Statistical analysis

Differences between groups with respect to means of tumor volume and radioactivity were evaluated by using Student's t-test.

3. Results and discussion

Liposomal size is an important factor for in vivo use; and, therefore, we firstly determined the size and zeta-potential of the liposomes prepared. As shown in Table 1, all liposomes used had similar characteristics except the non-modified liposomes, which showed a positive ζ-potential.

PEGylation has been widely applied, including polymer-conjugated photosensitizers, for PDT [14,15]. PEG-modification of liposomes avoids opsonization in the bloodstream, which is prerequisite for the clearance of the liposomes by reticuloendothelial system such as liver and spleen. As opsonized liposomes tend to make aggregates in the presence of serum [16], we determined the agglutinability of liposomes encapsulating BPD-MA in the presence of serum. PEG-Lip, APRPG-PEG-Lip, and Cont-lip with or without BPD-MA did not show any increase in turbidity in the presence of 50% serum, suggesting that these liposomes would not make large aggregates in the bloodstream (data not shown).

The feature of long-circulation causes enhanced accumulation of such drugs and carriers in tumor tissues, because the angiogenic vasculature in tumor tissue is quite leaky and macromolecules easily accumulate in the interstitial tissues of the tumor due to the enhanced permeability and retention (EPR) [17,18]. At first, we examined the biodistribution of BPD-MA in tumor tissue at 3 h after the intravenous injection of liposomal BPD-MA (Fig. 1). PEG-Lip BPD-MA and APRPG-PEG-Lip BPD-MA showed higher accumulation in the tumor tissue than did the Cont-Lip BPD-MA. These results are consistent with those of a previous study in which the biodistribution of PEG- and APRPG-PEG-modified liposomes was determined with radio-labeled cholesteryl oleoyl ether that had been incorporated into the liposomes; although the liposomal composition was different from that in the present work, as they were composed of distearoyl PC and cholesterol with DSPE-PEG or DSPE-PEG-APRPG (10:5:1) [12]. The

Table 1
Size and ζ-potential of PEG and APRPG-PEG liposomes

Liposomes	ζ-potential (mV)	Particle size (nm)
Cont-Lip BPD-MA	7.44±5.15	131.2±2.3
PEG-Lip BPD-MA	−7.69±6.80	151.4±3.5
APRPG-PEG-Lip BPD-MA	5.82±2.9	135.7±1.9

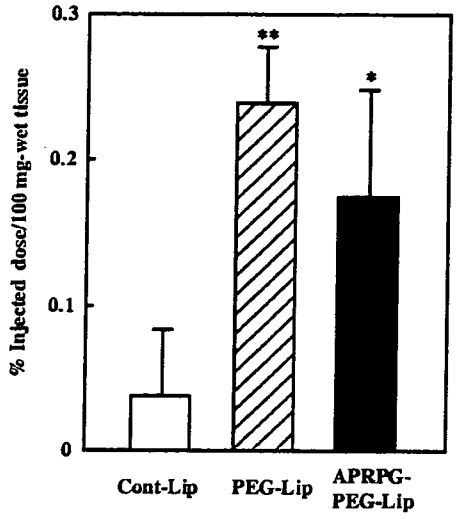

Fig. 1. Biodistribution of BPD-MA in tumor tissue after the injection of liposomal BPD-MA. Liposomal BPD-MA was injected into a tail vein of 5-week-old BALB/c male mice (n=4 or 5); and 3 h after the injection, BPD-MA in the tumor tissue was extracted and quantified by HPLC as described in Section 2. Date shows the percentages of the injected dose per 100 mg tissue and S.D. Significant difference against Cont-Lip, *P<0.05, **P<0.01.

previous study also indicated that APRPG-PEG-modified liposomes accumulated in tumor tissue significantly more than PEG-modified liposomes 24 h after the injection, although differential accumulation between the 2 formulations was not observed 1 h after injection of the liposomes. Here, we did not observe significant difference between the accumulation of PEG-Lip BPD-MA and that of APRPG-PEG-Lip BPD-MA 3 h after the injection. We speculate that the active targeting effected by APRPG modification would be clearly observed at time points later than 3 h.

Next we determined the tumor growth suppression after PDT by using Meth-A sarcoma-bearing mice. Targeting of angiogenic vasculature of tumors is promising for cancer treatment. Recently, antiangiogenic PDT has become a focus of interest. Tumor localization of the photosensitizer is an important key that determines PDT efficacy. Therefore, the improvement of PDT scheduling and the carrier of the photosensitizer for targeting to the angiogenic vasculature is important. In terms of PDT scheduling, in an earlier study, we showed that laser irradiation at a short time such as 15 min after the injection of photosensitizer was antiangiogenic PDT [7]. Actually, Dolmans and coworkers demonstrated that a photosensitizer was distributed to vascular endothelial cells to a greater extent at 15 min after the injection than at 4 h post injection, as determined by intravital microscopy [19,20]. As the antiangiogenic PDT would possibly damage blood cells, in this experiment, we applied laser irradiation 3 h after the injection of liposomes encapsulating BPD-MA. Moreover, APRPG-PEG-Lip BPD-MA would be expected to accumulate in angiogenic endothelial cells 3 h after the injection, since the liposomes would be actively targeting these cells.

The data from the therapeutic experiments indicated that APRPG-PEG-Lip BPD-MA significantly suppressed tumor growth and prolonged life (Fig. 2). On the contrary, consistent with our previous results [9], PEG-Lip BPD-MA showed only little suppression of tumor growth and no increase in the survival time of the tumor-bearing mice. The ineffectiveness of PEG-Lip BPD-MA for 3-h PDT may be explained as follows: PEG-modified liposomes were present in the interstitial tissue and produced singlet oxygen there, since PEG-modified liposomes did not interact strongly with either endothelial or tumor cells. In the case of PDT, the total amount of photosensitizer in the tumor tissue is not the important factor; rather the amount of it taken up in target cells during the time interval between the injection of the photosensitizer and the laser irradiation is critical. Therefore,

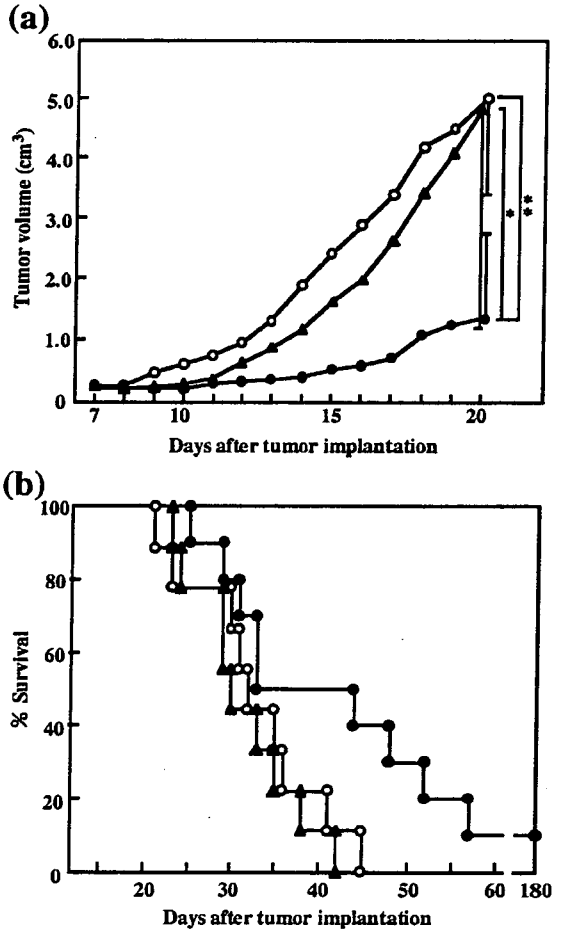

Fig. 2. Therapeutic experiment after PDT treatment with APRPG-PEG-modified liposomal BPD-MA. BALB/c mice were implanted subcutaneously into the left posterior flank with 1×10^6 Meth-A sarcoma cells. At day 7 after tumor implantation, saline (O), PEG-Lip BPD-MA (▲) or APRPG-PEG-Lip BPD-MA (●) was intravenously injected. At 3 h after the injection, the liposomal BPD-MA (0.5 mg/kg as BPD-MA)-treated mice were exposed to the laser light (689 nm, 150 J/cm^2) under pentobarbital anesthesia. Tumor volume (a) and survival (b) were monitored thereafter. Data points represent the mean±S.D. (n=9 or 10); and S.D. bars are shown only at day 20 for the sake of graphic clarity. *P<0.05, **P<0.01 for bracketed comparisons.

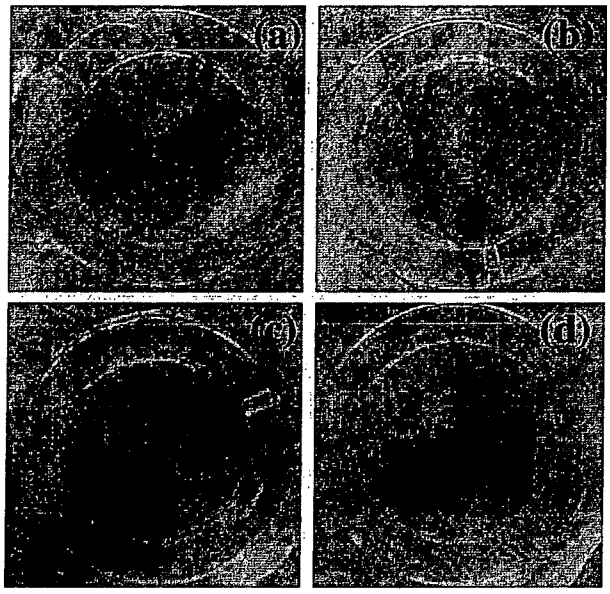

Fig. 3. Neovascular destruction following PDT treatment at 3 h post i.v. injection with APRPG-PEG-modified liposomal BPD-MA into angiogenesis-model mice. A Meth-A sarcoma (1×10^7 cells)-loaded chamber ring was implanted s.c. into each of several BALB/c mice. At day 4 after the implantation, PDT treatment was performed by an i.v. injection of saline (a), non-modified liposomal BPD-MA (0.5 mg/kg in terms of BPD-MA) (b), PEG-Lip BPD-MA (c), or APRPG-PEG-Lip BPD-MA (d). The animals (b–d) were exposed to a laser light of 689 nm with 150 J/cm^2 of fluence at 3 h post injection of the liposomal BPD-MA. At 24 h after PDT treatment, the mice were sacrificed; and the neovascularized dorsal skin was then resected for observation. Each group consisted of 3 mice and the pictures of each group were quite similar each other, although we presented a typical picture for each group.

active-targeting technology is quite useful, especially the targeting of angiogenic endothelial cells rather than tumor cells, since the damage to angiogenic endothelial cells would eradicate tumor cells through the cut off of oxygen. However, in the case of chemotherapy, PEG liposomes are widely used, because, in this case, slow and sustained release of chemotherapeutic agents at the tumor site is favorable. To enhance the interaction between carriers of photosensitizer and target cells, we previously prepared polycation liposomes as BPD-MA carrier for antiangiogenic PDT [21,22]. Polycation liposomes cause strong suppression of tumor growth when used for antiangiogenic PDT due to the strong electrostatic adhesion between the polycation and the plasma membrane of the vascular endothelial cell.

Finally, we observed actual vasculature damage caused by antiangiogenic PDT by the use of dorsal air sac-model mice. As shown in Fig. 3, only APRPG-PEG-Lip BPD-MA caused hemorrhage after 3-h PDT. Such vasculature damage might cause hemostasis, with the tumor cells being damaged by the lack of oxygen, in an actual tumor tissue.

In the present study we used APRPG-PEG-modified liposomes, although other attempts have been made to target angiogenic endothelial cells. Most of them were aimed at delivering chemotherapeutic agents to the cells and thereby indirectly eradicating tumor cells through damage to angiogenic vessels, namely, antineovascular chemotherapy. Those active-targeting techniques may also be useful for antiangiogenic PDT. Pastorino and coworkers reported on NGR peptide-modified long-circulating liposomes [23]. NGR peptide targets aminopeptidase N on angiogenic endothelial cells. Schiffelers and coworkers used RGD peptide-modified PEG liposomes [24]. RGD specifically binds integrin $\alpha v\beta 3$ that expressed on angiogenic endothelial cells. Angiogenic endothelial cell-expressed membrane type-1 matrix metalloproteinase (MT1-MMP) is also used as a target for antineovascular therapy, in which case, GPLPLR peptide-modified liposomes were used [25].

Taken together, active targeting, but not passive targeting, is useful for delivering photosensitizers for PDT, since the drugs not only would be delivered to the target tissue but also should be taken up by the target cells in a short period of time for the purpose of PDT. Furthermore, antiangiogenic PDT is a promising modality for cancer treatment.

Acknowledgements

This work was supported in part by a Grant-in-Aid for Scientific Research from the Japan Society for the Promotion of Science.

References

[1] A.Z. Dudek, W.Z. Pawlak, M.N. Kirstein, Molecular targets in the inhibition of angiogenesis, Expert Opin. Ther. Targets 7 (2003) 527–541.
[2] K. Shimizu, N. Oku, Cancer anti-angiogenic therapy, Biol. Pharm. Bull. 27 (2004) 599–605.
[3] V.H. Fingar, P.K. Kik, P.S. Haydon, P.B. Cerrito, M. Tseng, E. Abang, T.J. Wieman, Analysis of acute vascular damage after photodynamic therapy using benzoporphyrin derivative (BPD), Br. J. Cancer 79 (1999) 1702–1708.
[4] Y. Takeuchi, K. Kurohane, K. Ichikawa, S. Yonezawa, M. Nango, N. Oku, Induction of intensive tumor suppression by anti-angiogenic photodynamic therapy using polycation-modified liposomal photosensitizer, Cancer 97 (2003) 2027–2034.
[5] T.J. Dougherty, C.J. Gomer, B.W. Henderson, G. Jori, D. Kessel, M. Korbelik, J. Moan, Q. Peng, Photodynamic therapy, J. Natl. Cancer Inst. 90 (1998) 889–905.
[6] K. Ichikawa, Y. Takeuchi, S. Yonezawa, T. Hikita, K. Kurohane, Y. Namba, N. Oku, Antiangiogenic photodynamic therapy (PDT) using Visudyne causes effective suppression of tumor growth, Cancer Lett. 205 (2004) 39–48.
[7] K. Kurohane, A. Tominaga, K. Sato, J.R. North, Y. Namba, N. Oku, Photodynamic therapy targeted to tumor-induced angiogenic vessels, Cancer Lett. 167 (2001) 49–56.
[8] T. Ishida, H. Harashima, H. Kiwada, Liposome clearance, Biosci. Rep. 22 (2002) 197–224.
[9] K. Ichikawa, T. Hikita, N. Maeda, Y. Takeuchi, Y. Namba, N. Oku, PEGylation of liposome decreases the susceptibility of liposomal drug in cancer photodynamic therapy, Biol. Pharm. Bull. 27 (2004) 443–444.
[10] N. Oku, T. Asai, K. Watanabe, K. Kuromi, M. Nagatsuka, K. Kurohane, H. Kikkawa, K. Ogino, M. Tanaka, D. Ishikawa, H.